

Inkjet-Printed Conductive ITO Patterns for Transparent Security Systems

Evgeniia Gilshtein,* Sami Bolat, Galo Torres Sevilla, Antonio Cabas-Vidani, Frank Clemens, Thomas Graule, Ayodhya N. Tiwari, and Yaroslav E. Romanyuk*

Indium tin oxide (ITO) is a transparent conducting material that is widely used in devices where high transparency of the electrodes is required, such as flat panel and liquid crystal displays, touch panels, smart windows, and many others. ITO layers are deposited on a large scale by magnetron sputtering and then structured by lithography to define desired patterns of transparent electrodes. Here, a method for direct printing of transparent conductive patterns from ITO nanoparticle ink is communicated. The method combines inkjet printing with fast flash lamp annealing whereby the main novelty is to use an additional layer of a colored organic dye onto printed ITO to increase light absorption. The dye coating is instantly heated together with the underlying ITO layer by a light pulse, leading to an instant rise of the surface temperature, which is translated into improved optoelectronic properties of the ITO layers. Inkjet-printed ITO patterns processed with the dye-assisted flash lamp annealing exhibit a transmittance of up to 88% at 550 nm and resistivity of $3.1 \times 10^{-3} \Omega \text{ cm}$. Transparent touch-sensing trackpad and capacitive touch sensors are demonstrated based on the printed ITO patterns, which can be utilized in transparent security systems and other transparent Internet-of-Things devices.

Transparent conducting oxides (TCOs) based on wide-bandgap oxide semiconductors like $\text{In}_2\text{O}_3\text{:Sn}$ (ITO), $\text{SnO}_2\text{:F}$ (FTO), ZnO:Al (AZO) are indispensable components for optoelectronic devices where transparency of electrodes is required. Some examples are solar cells, energy-efficient and switchable windows, touch panels, and liquid crystal displays.^[1,2] Among various TCO materials, indium tin oxide (ITO) is the most prominent due to its low electrical resistivity in conjunction with high transmittance in the


visible range. Magnetron sputtering is used on an industrial scale to fabricate high-performance ITO films with resistivity values down to $10^{-5} \Omega \text{ cm}$.^[3–5] In research, many efforts have been devoted to synthesizing ITO films by solution-based processes such as spray pyrolysis, dip-coating, spin-coating, and casting.^[6–9] The use of crystalline nanoparticles (NPs) is also possible for ink-based techniques since individual ITO NPs were found to have a resistivity as low as $2 \times 10^{-4} \Omega \text{ cm}$.^[10] One practical advantage of ink-based processes is the possibility of direct patterning of ITO structures, which can be achieved by digital printing of ITO-containing inks. Thus, ITO patterns have been prepared by inkjet^[11–17] or gravure printing^[18–20] endowing fast, simple, and high-throughput printable optoelectronics.^[19–23] Inkjet-printed NPs-based ITO films have demonstrated resistivity values on the order of $10^{-2} \Omega \text{ cm}$; however, they required postdeposition annealing at the temperatures higher than 300 °C for about

6 h.^[19] This makes them incompatible with many intended low-temperature device stacks and temperature-sensitive substrates.

In this work, we investigate inkjet printing of an ITO nanoparticle ink in combination with flash lamp annealing to obtain conductive and transparent patterns. This annealing step is crucial for improving the layer density and composition that enables high carrier mobility.^[24,25] Flash lamp annealing (FLA), also known as intense pulsed light (IPL) or photonic curing (PC), employs ultrashort (0.1 to 10 ms) pulses from a xenon flash lamp to induce rapid, transient heating of illuminated surfaces. This process allows fast annealing, drying, or sintering of thin films with a higher throughput when compared to conventional methods while allowing the use of temperature-sensitive substrates.^[26] FLA is often used for annealing of opaque materials and metal films, such as printable Ag, Cu, or carbon-based inks,^[27,28] due to higher absorbance of radiant lamp energy by such films. However, as the emission spectrum of a xenon lamp has a maximum in the visible region, it is difficult to process optically transparent films. Thereby, our approach is to apply organic coloring agent (dye) onto printed ITO films in order to increase light absorption and, therefore, to intensify the sintering of the ITO film. It was found that the electrical resistivity of inkjet-printed ITO films could be significantly reduced thanks to the effective annealing of the ITO films. As possible applications, we demonstrate inkjet-printed

Dr. E. Gilshtein, S. Bolat, Dr. G. T. Sevilla, A. Cabas-Vidani, Prof. A. N. Tiwari, Dr. Y. E. Romanyuk
Laboratory for Thin Films and Photovoltaics
Empa-Swiss Federal Laboratories for Materials Science and Technology
Überlandstrasse 129, Dübendorf 8600, Switzerland
E-mail: evgeniia.gilshtein@empa.ch; yaroslav.romanyuk@empa.ch

Dr. F. Clemens, Prof. T. Graule
Laboratory for High Performance Ceramics
Empa-Swiss Federal Laboratories for Materials Science and Technology
Überlandstrasse 129, Dübendorf 8600, Switzerland

 The ORCID identification number(s) for the author(s) of this article can be found under <https://doi.org/10.1002/admt.202000369>.

© 2020 Empa. Published by WILEY-VCH Verlag GmbH & Co. KGaA, Weinheim. This is an open access article under the terms of the Creative Commons Attribution License, which permits use, distribution and reproduction in any medium, provided the original work is properly cited.

DOI: 10.1002/admt.202000369

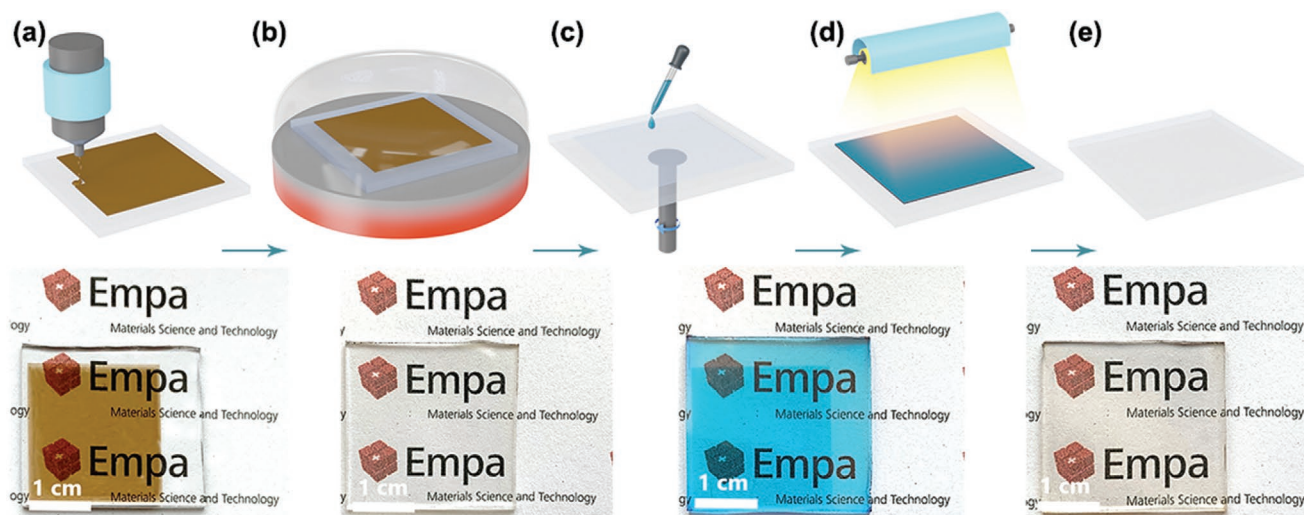


Figure 1. Schematic illustration of the fabrication process with corresponding sample photographs: a) inkjet printing of ITO layer; b) vacuum annealing of ITO film; c) spin-coating of Sensitizer dye on top of the annealed ITO film; d) flash lamp annealing of the ITO film with the dye on top; e) processed ITO layer on glass.

ITO-based transparent devices such as a transparent touch-sensing trackpad and a transparent capacitive touch sensor, which can be used in transparent security systems.

Figure 1 schematically describes the fabrication steps of conductive ITO patterns. ITO nanoink is inkjet-printed on the soda-lime glass (SLG) substrate. A series of ITO films were also fabricated via a spin-coating method to assess their optoelectrical properties. Due to the presence of the cyclododecene solvent and ink stabilizers, as-printed ITO films are brown and nonconductive (Figure 1a). After annealing in a low vacuum (0.1 Pa) for 1 h at 250 °C (Figure 1b), the precursor film becomes transparent. As the next step, the dispersion of a blue organic dye (Sensitizer SQ2) in ethanol is spin-coated onto the ITO film (Figure 1c). ITO film with the dye layer is then processed with FLA (Figure 1d). After the FLA step, the ITO film becomes transparent again (Figure 1e) because the dye layer, acting as the light absorber, decomposes during the FLA. The detailed experimental conditions are described in the Experimental Section.

The average size of ITO nanoparticles (inset of **Figure 2a**) is around 5 nm, as seen from the scanning electron microscopy

(SEM) image (Figure 2a). Thermal analysis curves for the brown-colored ITO ink are shown in Figure 2b. The thermogravimetric analysis (TGA) curve has only a single step with a weight loss of 17.1% between 220 and 290 °C, corresponding to the decomposition of the solvent and removal of organic impurities. The sintering of ITO nanoparticles accompanies this process, which is reflected by a broad endothermic peak on the differential scanning calorimetry (DSC) curve. Based on the DSC curve, 250 °C was selected as an optimal annealing temperature.

The initial low-vacuum annealing step at 250 °C is performed to obtain an as-prepared transparent ITO thin film on SLG. The SEM planar view shown in Figure 2c presents a densely packed structure of the as-prepared ITO layer, whereas the inset of Figure 2c exhibits a cross-sectional image of the ITO layer. Due to the high solid loading of the ink (20% wt), the film is uniform and crack-free. The thickness of the spin-coated layer is in the range 70–80 nm, whereas, for inkjet-printed ITO layers, the thickness is around 200 and 500 nm for one and two printing cycles, respectively. After the optimization of all printing parameters, ITO patterns with a size of 2.5 mm × 2.5 mm were

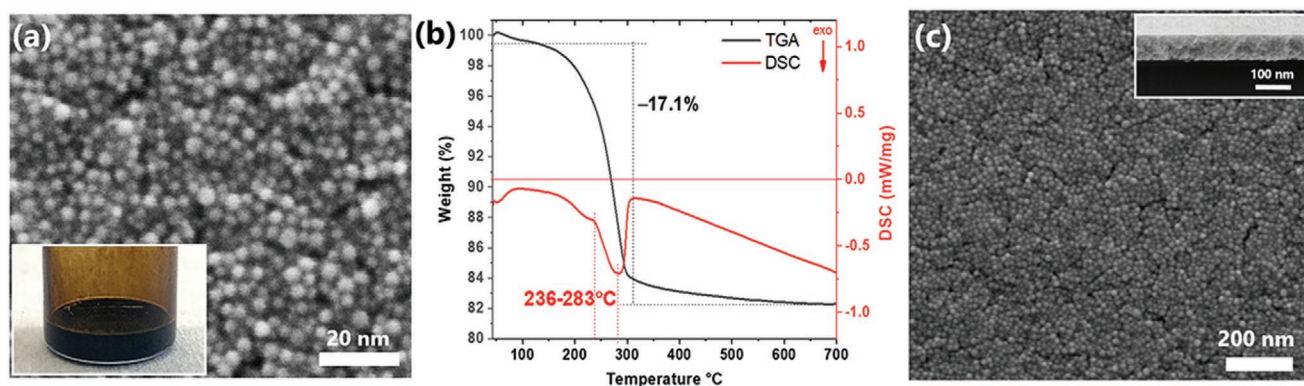


Figure 2. a) SEM image of ITO nanoparticles from nanoink solution (inset image); b) DSC and TGA curves for the ITO ink. c) Top-view and (inset) cross-sectional SEM images of as-prepared ITO film after the initial low-vacuum annealing step.

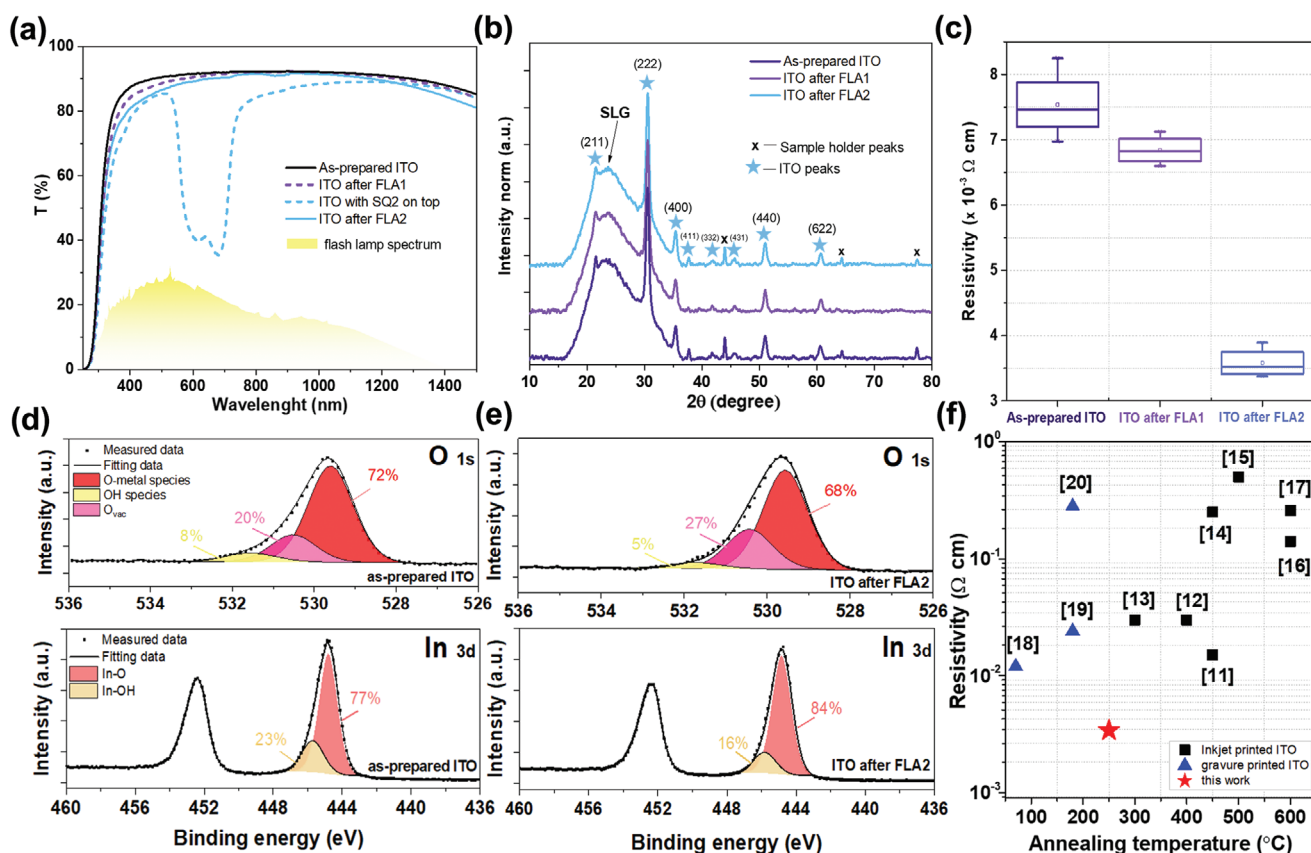


Figure 3. Characterization of the ITO films at different annealing stages. a) Optical transmittance curves; b) XRD patterns; c) resistivity of the ITO films; d) O 1s and In 3d XPS peaks deconvolution after the low vacuum annealing step; e) O 1s and In 3d XPS peaks deconvolution after dye-assisted FLA; f) resistivity for the reported printed ITO films versus applied temperature during the annealing process.

printed with different printing resolutions. The resolution of 400 dpi was found to be optimum for continuous and homogeneous layers (Figure S1, Supporting Information).

The 70 nm thick as-prepared ITO film on SLG has a transmittance ($T\%$) of 80–92% in the broad wavelength range of 380–1100 nm (Figure 3a). In order to analyze the flash lamp treatment effect, two consecutive FLA treatments are applied on an as-prepared ITO film (hereafter called FLA1) and on the ITO layer with the SQ2 dye (hereafter called FLA2). FLA1 results in a slight reduction of the transmittance value of the ITO structure in the visible range (black line for as-prepared ITO compared to the dashed violet line — for ITO after FLA1). After depositing the SQ2 dye onto the ITO layer, a significant drop in transmittance is observed within 500–750 nm, which is associated with the SQ2 dye absorption (dashed blue line). The SQ2 mentioned above exhibits a broad absorption band in the 510–750 nm region with a maximum at 650 nm.^[29] Since the emission spectrum of the xenon lamp^[30] (Figure 3a) has a broad peak in the visible region (400–800 nm), FLA2 is applied on the dye-covered ITO layer resulting in the removal of the dye absorption peak (blue line). We assume that after the pulsed light absorption, the dye layer is instantly heated together with the underlying ITO layer. This leads to its thermal decomposition and evaporation of the decomposition products from the surface. FLA performed in the air ambient is known to result in a fast decomposition of the precursors assisted by oxidation.^[31]

For the as-prepared ITO film, diffraction reflexes 211, 222, 400, 440, and 622 can be observed, where the 222 reflex has the maximum intensity (Figure 3b). This pattern matches well with the diffraction pattern of cubic crystalline ITO.^[25,32] Similar patterns are observed for the ITO film after the initial FLA1 and for the film after application of the dye layer and subsequent FLA2. Based on the simulated temperature profiles (Figure S2, Supporting Information), the surface temperature after FLA2 is rising to the level of 600 °C, and diffraction reflections of the cubic ITO structure are visible. It has been shown for RF magnetron sputtered ITO films^[33] as well as for synthesized ITO nanoparticle films,^[34,35] that after applying annealing temperatures in the range of 300–600 °C the diffraction reflections of cubic ITO structure appear. Thus, the crystalline structure remains unchanged for the ITO films independently from the applied annealing process.

Figure 3c shows the resistivity of ITO films as a function of the applied annealing process. The FLA1 step on as-prepared ITO film results in an insignificant drop in resistivity, indicating that the heating of the ITO film during FLA1 is not sufficient for conductivity improvement. Application of the FLA2 step to the dye-coated ITO film results in the decrease of the resistivity by a factor of 2. One can assume that higher temperatures are obtained on the surface of the ITO film due to the increased absorption by the dye layer.^[36] In order to prove this assumption, the temperature simulations were carried out with the SimPulse software. According to simulations (Figure S2,

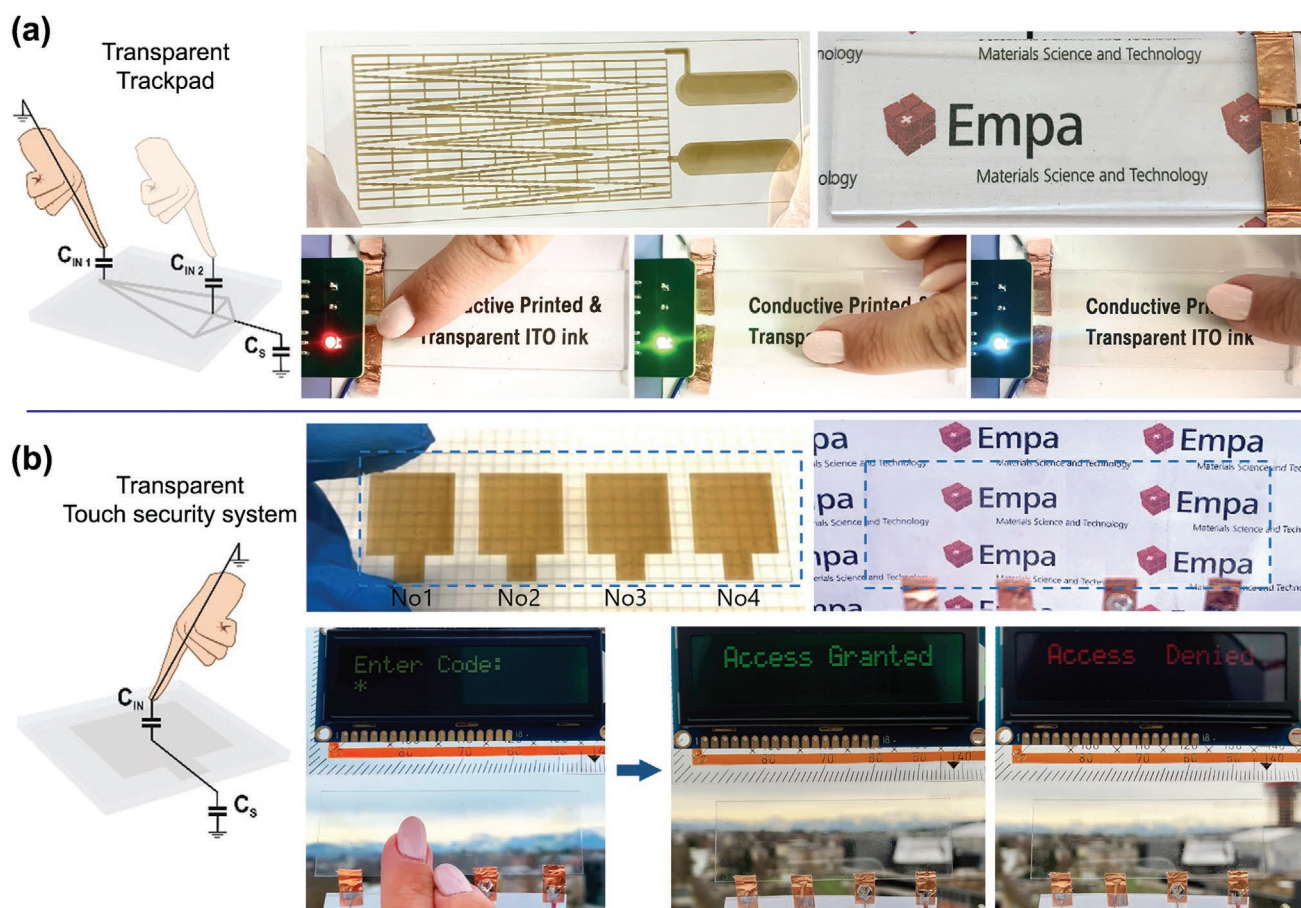


Figure 4. Application of transparent and conductive ITO patterns in a) transparent touch-sensing trackpad and b) capacitive touch sensor for security system. The patterns of trackpad and capacitive touch sensors are inkjet-printed and annealed following the steps described in this study. When the trackpad is touched, movements of the user's finger can be visualized through the red (left corner position), green (middle position), and blue (right corner position) colors. The capacitive touch sensor was operated by exact sensing through the four ITO electrodes assigned to "1, 2, 3, 4" numbers. By consequent pressing of the ITO electrodes by the finger, the user gets "Access Granted" or "Access Denied" messages on the LCD depending on the input.

Supporting Information), the presence of the SQ2 dye elevates the surface temperature of the ITO film up to 600 °C during FLA pulses that last for 0.2 ms each.

The amount of the dye left on the surface of the ITO after FLA is not significant, which is confirmed by the X-ray photoelectron spectroscopy (XPS) surveys (Figure S3, Supporting Information) for the as-prepared ITO layer and the layer after FLA2. After the dye-assisted FLA2 step, the amount of $-OH$ species decreases (Figure 3d,e). This is confirmed from both O 1s (from 8% to 5%) and In 3d (from 23% to 16%) detailed peaks at 531.7 and 445.7 eV,^[32,37] respectively. On the contrary, the amount of defected oxygen states or vacancies (O_{vac}) associated with the 530.4 eV peak increases from 20% to 27%, which correlates with the increased carrier density in the ITO film.^[32] As a result, the electron Hall mobility and carrier concentration of the ITO films are $2.9 \text{ cm}^2 \text{ V}^{-1} \text{ s}^{-1}$ and $5.7 \times 10^{-20} \text{ cm}^{-3}$, respectively. The lowest resistivity value of $3.1 \times 10^{-3} \Omega \text{ cm}$ obtained in our work is about one order of magnitude lower than those reported for the gravure or inkjet-printed ITO layers (Figure 3f). Important electrical parameters of the fabricated ITO layers are also summarized in Table S1 (Supporting Information). The annealing temperature for the gravure printed

ITO layers was as low as 70 °C;^[18] however, the resistivity of the samples was only $1.2 \times 10^{-2} \Omega \text{ cm}$. The previously reported inkjet-printed ITO layers required annealing temperatures higher than 300 °C, and their electrical resistivity could not be lowered below $10^{-2} \Omega \text{ cm}$ ^[11–17] (Figure 3f).

In order to utilize unique features of printed conductive ITO patterns, several device prototypes were fabricated, such as a transparent trackpad (Figure 4a) and a touch sensor for the transparent security systems (Figure 4b). The structure of the trackpad was inkjet-printed from the ITO ink and processed by the dye-assisted FLA method described previously. When the trackpad is touched (Figure 4a), signals are processed so that movements of the user's finger on the trackpad can be visualized immediately through the corresponding LED colors, depending on the finger position. Figure 4b demonstrates the multiple touchpoint operation of a transparent capacitive-type sensor based on printed ITO. The detailed operation principles of both systems are described in the Supporting Information, and the demonstrations are shown in Video S1 (Supporting Information).

To summarize, an innovative approach for printing highly conductive and transparent ITO patterns is proposed, which is based on flash lamp annealing of dye-sensitized ITO precursor

films. Due to the increased light absorption, it is possible to obtain higher surface temperatures, enabling the sintering of ITO nanoparticle-based layers and reducing the hydroxide content. The inkjet-printed ITO film annealed at 250 °C and processed with the FLA exhibit a visible transmittance of up to 88% and a resistivity as low as $3.1 \times 10^{-3} \Omega \text{ cm}$. Printed and processed transparent ITO electrodes can be utilized for security systems and other Internet-of-Things electronic applications. The proposed dye-integrated process can potentially be extended to other transparent materials and be processed on temperature-sensitive substrates.

Experimental Section

Materials: NPs-based ITO ink with 20 wt% concentration in cyclododecene and 6.3 mPa s viscosity from ULVAC, Inc. and blue dye Sensitizer SQ2 from Solaronix were used in this study. Sensitizer SQ2 is a purely organic sensitizer that is widely used to enhance the photovoltaic performance of dye-sensitized solar cells^[38] due to its incident photons absorption.

Fabrication and Annealing: Spin-coating of the ITO ink was performed at room temperature, with a rotation speed of 3500 rpm min⁻¹ and a duration of 25 s, resulting in a 70–80 nm thick ITO layer. SLG with a thickness of 1 mm and a size of 2.5 cm × 2.5 cm were used as substrates. They were cleaned in a consequential order with 10% diluted acetic acid, isopropanol, and deionized (DI) water, followed by subsequent oxygen plasma cleaning for 2 min to improve surface wettability. After the spin-coating step, the films were annealed at 250 °C in a tube furnace under low vacuum (0.1 Pa) conditions for 1 h. Inkjet printing was performed with a Meyer Burger PixDRO LP50 inkjet printer by using Dimatix disposable cartridges with 10 pL nozzle volume (native resolution 100 dpi). Detailed information on the inkjet printing process is described in the Supporting Information. In order to obtain the necessary wetting of the SLG substrate, O₂ plasma treatment for 2 min was applied before the printing step. The postdeposition annealing conditions for the inkjet-printed samples were the same as for the spin-coated layers. After one printing cycle, the ITO pattern thickness was around 200 nm.

Blue dye Sensitizer SQ2 from Solaronix was spin-coated onto the ITO patterns with a speed of 1500 rpm min⁻¹ and a duration of 15 s from $4.5 \times 10^{-3} \text{ M}$ solution in ethanol. FLA of the ITO patterns was performed in the air atmosphere with a photonic curing system (NovaCentrix PulseForge 1300). For the FLA processes, samples were positioned 10 mm away from a Xe arc lamp with the face of the ITO pattern directed toward the incident light. One pulse light consisted of 1000 μs pulse envelope comprised of three 280 μs micropulses with an 80 μs break after each. Repeating the FLA treatment leads to the improvement of the FLA-processed ITO optoelectrical properties. Therefore, consequent annealing steps of ITO patterns, using 700 V lamp voltage with ten pulses repetition (50 J cm⁻² total output energy density), 800 V—10 more pulses (70 J cm⁻²) and 900 V—30 more repetitions (300 J cm⁻²) with the same pulse parameters were applied. These pulse parameters and repetition numbers were extracted after a series of experiments until ITO patterns exhibited stable and unchanged sheet resistance values. Additional information on the FLA processes is described in the Supporting Information.

Characterization: TGA and DSC on NPs brown-colored dispersion were performed with a Netzsch STA 449 F3 Jupiter in a temperature range from room temperature to 700 °C at a ramping speed of 5 °C min⁻¹. Thickness values for both spin-coated and inkjet-printed layers were obtained from SEM measurements (FEI Quanta 650 SEM). Transmittance was measured with a UV-vis spectrometer Shimadzu UV-3600 from 250 to 1500 nm taking air as the reference (baseline). Electrical properties of annealed layers were measured by Hall effect measurement on ECOPIA HMS3000 apparatus using the van der Pauw contacting configuration with gold contacts. X-ray diffraction (XRD)

patterns for thin films were recorded with a grazing incidence angle of 1.5°, a step size of 0.04°, and a scan rate of 0.5 s step for 2 θ angle scan from 10 to 80 using a Bruker D8 diffractometer with Cu K α radiation. XPS measurements were performed using a Quantum2000 photoelectron spectrometer from Physical Electronics with a monochromatic Al K α source (1486.6 eV) and a base pressure below 8×10^{-9} mbar. Survey spectra were recorded with an energy step size of 0.4 eV and a pass energy of 93.90 eV. For depth profiling, detailed peak spectra were recorded with an energy step size of 0.125 eV and a pass energy of 29.35 eV. After the depth profile measurements of samples after different annealing steps, the composition of the samples was analyzed using the Multipak and CasaXPS software.

Supporting Information

Supporting Information is available from the Wiley Online Library or from the author.

Acknowledgements

The authors acknowledge funding from the Swiss National Science Foundation (SNF) (Grant No. IZLCZ2_170276/1) for a Sino-Swiss Science and Technology Cooperation project. The authors acknowledge financial support from the Strategic Focus Area Advanced Manufacturing of the ETH domain under the project FOXIP – Functional OXides Printed on Polymers and Paper. The authors also thank Gorjan Lovro for the TGA/DSC measurements and the financial supports for the instrument from the SNF project (Grant No. 206021_164024).

Conflict of Interest

The authors declare no conflict of interest.

Keywords

capacitive touch sensors, flash lamp annealing, indium tin oxide, inkjet printing, transparent electrodes

Received: April 18, 2020
Revised: June 24, 2020
Published online: July 29, 2020

- [1] T. Minami, *Semicond. Sci. Technol.* **2005**, *20*, S35.
- [2] D. S. Ginley, C. Bright, *MRS Bull.* **2000**, *25*, 15.
- [3] B. Parida, Y. Gil, H. Kim, *J. Nanosci. Nanotechnol.* **2019**, *19*, 1455.
- [4] M. G. Sousa, A. F. da Cunha, *Appl. Surf. Sci.* **2019**, *484*, 257.
- [5] P. Prepelita, I. Stavarache, D. Craciun, F. Garoi, C. Negrila, B. G. Sbarcea, V. Craciun, *Beilstein J. Nanotechnol.* **2019**, *10*, 1511.
- [6] S. Seki, Y. Sawada, M. Ogawa, M. Yamamoto, Y. Kagota, A. Shida, M. Ide, *Surf. Coat. Technol.* **2003**, *169*, 525.
- [7] J. Song, S. A. Kulinich, J. Li, Y. Liu, H. Zeng, *Angew. Chem., Int. Ed.* **2015**, *54*, 698.
- [8] R. M. Pasquarelli, D. S. Ginley, R. O'Hayre, *Chem. Soc. Rev.* **2011**, *40*, 5406.
- [9] Y. Liu, T. Moser, C. Andres, L. Gorjan, A. Remhof, F. Clemens, T. Graule, A. N. Tiwari, Y. E. Romanyuk, *J. Mater. Chem. A* **2019**, *7*, 3083.
- [10] J. Ederth, P. Hesler, A. Hultåker, G. A. Niklasson, C. G. Granqvist, *Thin Solid Films* **2003**, *445*, 199.

- [11] J. A. Jeong, J. Lee, H. Kim, H. K. Kim, S. I. Na, *Sol. Energy Mater. Sol. Cells* **2010**, 94, 1840.
- [12] M. S. Hwang, B. Y. Jeong, J. Moon, S. K. Chun, J. Kim, *Mater. Sci. Eng., B* **2011**, 176, 1128.
- [13] G. Bühler, D. Thölmann, C. Feldmann, *Adv. Mater.* **2007**, 19, 2224.
- [14] A. Olziersky, A. Vilà, J. R. Morante, *Thin Solid Films* **2011**, 520, 1334.
- [15] J. Yu, S. Lee, E. Lim, T. Kim, K. K. Lee, *Mol. Cryst. Liq. Cryst.* **2010**, 519, 134.
- [16] S. J. Hong, J. W. Kim, J. I. Han, *Curr. Appl. Phys.* **2011**.
- [17] S. J. Hong, J. W. Kim, J. W. Lim, G. S. Choi, M. Isshiki, *Mater. Trans.* **2010**, 51, 1905.
- [18] A. A. Serkov, H. V. Snelling, S. Heusing, T. M. Amaral, *Sci. Rep.* **2019**, 9, 1773.
- [19] J. Puetz, M. A. Aegerter, *Thin Solid Films* **2008**, 516, 4495.
- [20] S. Heusing, P. W. de Oliveira, E. Kraker, A. Haase, C. Palfinger, M. Veith, *Thin Solid Films* **2009**, 518, 1164.
- [21] H. Y. Lai, T. H. Chen, C. H. Chen, *Mater. Lett.* **2011**, 65, 3336.
- [22] J. A. Jeong, H. K. Kim, *Curr. Appl. Phys.* **2010**, 10, e105.
- [23] J. Maslik, I. Kuritka, P. Urbanek, P. Krcmar, P. Suly, M. Masar, M. Machovsky, *Sensors* **2018**, 18, 3246.
- [24] J. B. Plumley, A. W. Cook, C. A. Larsen, K. Artyushkova, S. M. Han, T. L. Peng, R. A. Kemp, *J. Mater. Sci.* **2018**, 53, 12949.
- [25] R. Ramadan, K. Abdelhady, M. Manso-Silván, V. Torres-Costa, R. J. Martín-Palma, *J. Photonics Energy* **2019**, 9, 034001.
- [26] L. Rebohle, *Flash Lamp Annealing: From Basics to Applications*, Springer International Publishing, Cham, Switzerland **2019**, pp. 15–70.
- [27] E. B. Secor, B. Y. Ahn, T. Z. Gao, J. A. Lewis, M. C. Hersam, *Adv. Mater.* **2015**, 27, 6683.
- [28] M. H. Yu, S. J. Joo, H. S. Kim, *Nanotechnology* **2017**, 28, 205205.
- [29] M. Klein, R. Pankiewicz, M. Zalas, W. Stampor, *Sci. Rep.* **2016**, 6, 30077.
- [30] S. Luo, S. Zhang, B. B. Bourgeois, B. C. Riggs, K. A. Schroder, Y. Zhang, J. He, S. Adireddy, K. Sun, J. T. Shipman, M. M. Oguntoye, V. Puli, W. Liu, R. Tu, L. Zhang, S. Farnsworth, D. B. Chrisey, *J. Mater. Res.* **2017**, 32, 1701.
- [31] M. Y. Jiang, Y. Q. Wu, G. S. Lin, L. J. Xu, Z. Chen, F. F. Fu, *Sci. Total Environ.* **2011**, 409, 4449.
- [32] T. Tohsophon, A. Dabirian, S. De Wolf, M. Morales-Masis, C. Ballif, *APL Mater.* **2015**, 3, 116105.
- [33] Q. Li, W. Mao, Y. Zhou, C. Yang, Y. Liu, C. He, *J. Appl. Phys.* **2015**, 118, 025304.
- [34] S. Manafi, S. Tazikeh, S. Joughehdoust, *Mater. Sci.-Poland* **2017**, 35, 799.
- [35] S.-J. Hong, J.-I. Han, *J. Electroceram.* **2006**, 17, 821.
- [36] J. Patwari, A. Chatterjee, S. Sardar, P. Lemmens, S. K. Pal, *Phys. Chem. Chem. Phys.* **2018**, 20, 10418.
- [37] M. T. Dang, J. Lefebvre, J. D. Wuest, *ACS Sustainable Chem. Eng.* **2015**, 3, 3373.
- [38] M. Younas, M. A. Gondal, U. Mehmood, K. Harrabi, Z. H. Yamani, F. A. Al-Sulaiman, *Int. J. Energy Res.* **2018**, 42, 3957.